Electronic Supplementary Information

Enhanced Thermoelectric Performance in Rare-earth Filled-skutterudites

Yulong Li,[a,b,c] Pengfei Qiu,[a,b] Haozhi Duan,[a,b,c] Jikun Chen,[a,b] G. Jeffrey Snyder,[d] Xun Shi,*[,a,b] Bo Brummerstedt Iversen*[,e] and Lidong Chen*[,a,b]

[a]State Key Laboratory of High Performance Ceramics and Superfine Microstructure, Shanghai Institute of Ceramics, Chinese Academy of Sciences, Shanghai 200050, China.
[b]CAS Key Laboratory of Materials for Energy Conversion, Shanghai Institute of Ceramics, Chinese Academy of Sciences, Shanghai, 200050, China.
[c]University of Chinese Academy of Sciences, Beijing 100049, China.
[d]Department of Materials Science and Engineering, Northwestern University, Evanston, Illinois 60208, USA.
[e]Center Materials Crystallography, Department of Chemistry and iNANO, Aarhus University, Langelandsgade 140, 8000 Aarhus C, Denmark.
Correspondence and requests for materials should be addressed to Xun Shi (email: xshi@mail.sic.ac.cn), Lidong Chen (email: cld@mail.sic.ac.cn), or Bo Brummerstedt Iversen (email: bo@chem.au.dk).

Structural Characterization

The SEM photographs and grazing-angle incidence X-ray diffraction (GIXD) patterns of the ribbons after MS are shown in Fig. S1. The side of the ribbons contacting with the copper wheel after MS is defined as 'contacting face'. Another side of the ribbons is defined as 'free face'. As shown in Fig. S1a, fine uniform crystal grains with the size below 200 nm are observed in the free face. The phases of these crystalline grains in the free face, identified by GIXD measurement with a 5° grazing angle (see Fig. S1c), are $CoSb_3$, $CoSb_2$, and Sb. Whereas, in the contacting face, the intensity of all the GIXD peaks is very weak (the peaks from 20-25° arise from the substrate during the measurement), indicating weak crystallization due to the ultrafast cooling rate on this side when the melt liquid contact the high-speed-rotated copper wheel. There is also almost no crystallization observed in the contacting face by SEM.

Figure S2 shows the X-ray diffraction patterns for $R_{0.2}Co_4Sb_{12}$ (R = Nd, Sm, Gd, Tb, Dy, and Tm) samples prepared by the NEMH process. The main phase for all the samples is $CoSb_3$ (JCPDS No. 65-3144). Some impurity diffraction peaks, which are identified as belonging to $CoSb_2$ and RSb phases, are observed in the X-ray diffraction patterns for filler Tm, Dy, Tb, and Gd.

Lattice parameters calculated by an analytical extrapolation function of $(\cos^2\theta/\sin\theta+\cos^2\theta/\theta)/2$ are shown in Fig. S3. The lattice parameters of these rare-earth filled $R_yCo_4Sb_{12}$ follow the similar increasing trend with Yb- or K-filled skutterudites, but lower than that of Ba- or Eu-filled skutterudites[1-5].

Low-temperature Thermal Conductivity

Figure S6 shows the low-temperature κ_L from 10 to 300 K for $CoSb_3$ and $R_yCo_4Sb_{12}$ (R = Nd, Sm, Gd, Tb, and Dy). Debye approximation is used to model the temperature dependence of the low-temperature κ_L for all the samples. In the Debye model[7,8], lattice thermal conductivity is given by

$$\kappa_L = \frac{k_B}{2\pi^2 v}\left(\frac{k_B}{\hbar}\right)^3 T^3 \int_0^{\theta_D/T} \frac{x^4 e^x}{\tau_c^{-1}\left(e^x-1\right)^2} dx. \quad \text{(S1)}$$

where $x = \hbar\omega / k_B T$, ω is the phonon frequency, k_B is the Boltzmann constant, $\hbar$ is the reduced Planck constant, θ_D is the Debye temperature, v is the velocity of sound, and τ_c is the phonon scattering relaxation time. The overall phonon scattering relaxation rate τ_c^{-1} is written as

$$\tau_c^{-1} = \frac{v}{L} + A\omega^4 + B\omega^2 T\, \mathrm{e}^{-\theta_D/3T} + \frac{C\omega^2}{(\omega_0^2 - \omega^2)^2}. \quad \text{(S2)}$$

where L is the grain size, A, B and C are the fitting parameters, and ω_0 is the resonance frequency. The terms on the right side of Eq. (S2) are the relaxation times for grain boundary scattering, point defect scattering, phonon-phonon Umklapp scattering and resonant phonon scattering, respectively. In our calculations, the Debye temperature (θ_D = 287 K) and the velocity of sound (v = 2700 m/s) are taken from literatures[9]. The fitted curves of low-temperature κ_L using Eq. (S1) and (S2) are plotted in Fig. S6. The solid lines fit the experimental data very well over the entire temperature range for all the samples. The fitted parameters are listed in Table S2.

The fitted grain size (L) varies from about 1 to 4 μm for all the samples, consistent well with the observations by Scanning Electron Microscope (SEM). The fitted parameter A for point defect scattering increases monotonously with increasing filling fractions (y) due to the enhanced phonon-point defect scattering when the fillers insert into $CoSb_3$ lattice. For Umklapp scattering, the parameter B is around 3.5×10^{-18} s/K for all the samples and no obvious trend as a function of y is observed. For resonant phonon scattering, the parameter C is proportional to the concentration of resonant scattering center formed by the fillers in the voids of $CoSb_3$ lattice, and ω_0 is the resonant frequency of the fillers.

Supplementary Figures and Tables

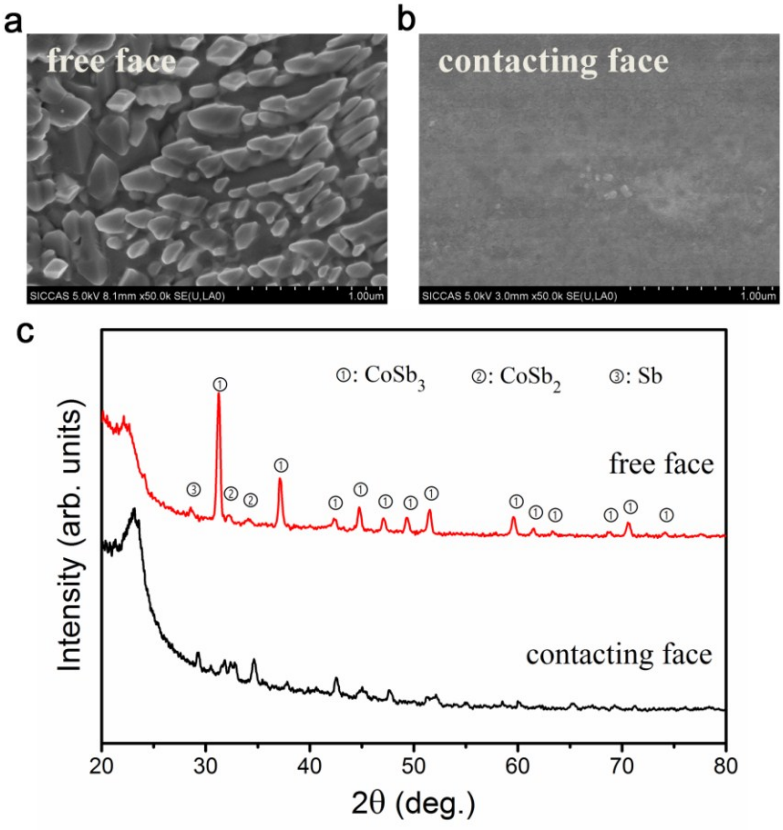

Fig. S1 SEM photographs of the ribbons after MS: (a) free face and (b) contacting face, as well as (c) GIXD patterns for the ribbons after MS.

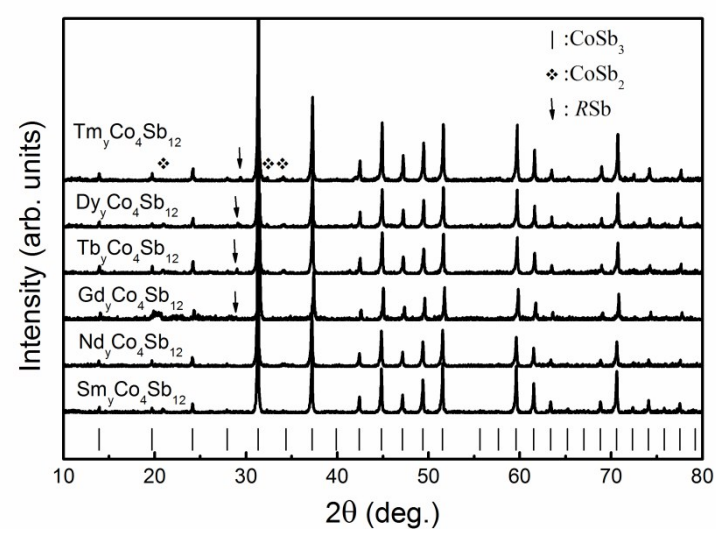

Fig. S2 XRD patterns for $R_yCo_4Sb_{12}$ (R = Nd, Sm, Gd, Tb, Dy, and Tm) prepared by the NEMH method.

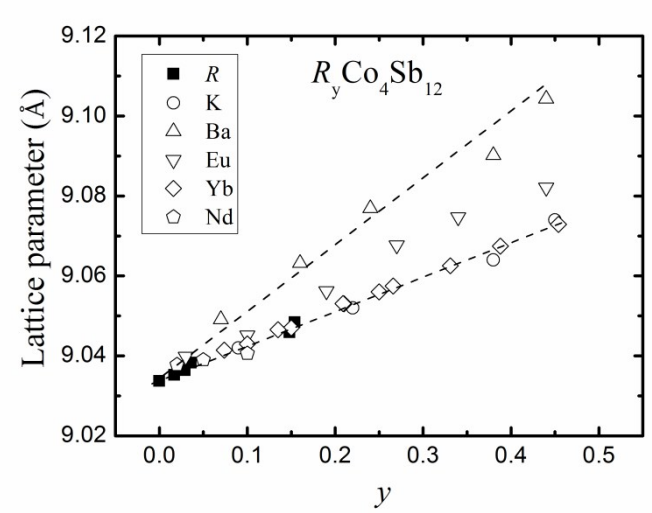

Fig. S3 Lattice parameter as a function of actual filling fraction y for $R_yCo_4Sb_{12}$ (R represents the fillers: Nd, Sm, Gd, Tb, Dy, and Tm)[1-6]. The dashed lines are guides to the eyes.

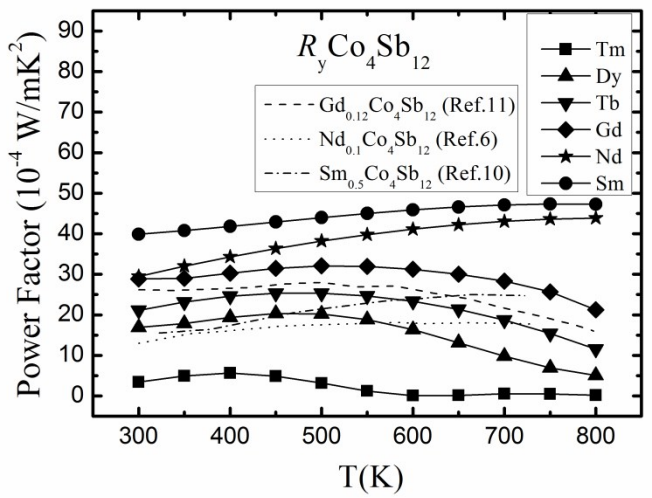

Fig. S4 Temperature dependence of power factor for $R_yCo_4Sb_{12}$ (R = Nd, Sm, Gd, Tb, Dy, and Tm). The data for the Nd-filled sample prepared by TMQA method, and the Gd- and Sm-filled samples prepared by HP method are included for comparison[6,10,11].

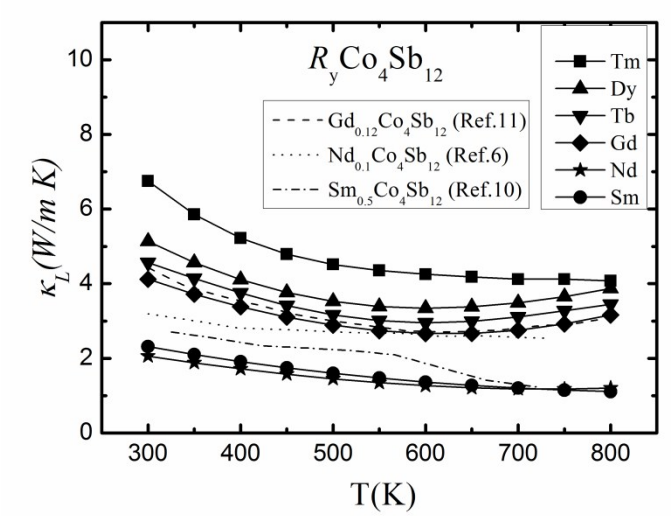

Fig. S5 Temperature dependence of lattice thermal conductivity κ_L for $R_yCo_4Sb_{12}$ (R = Nd, Sm, Gd, Tb, Dy, and Tm). The data for the Nd-filled sample prepared by TMQA method, and the Gd- and Sm-filled samples prepared by HP method are included for comparison[6,10,11].

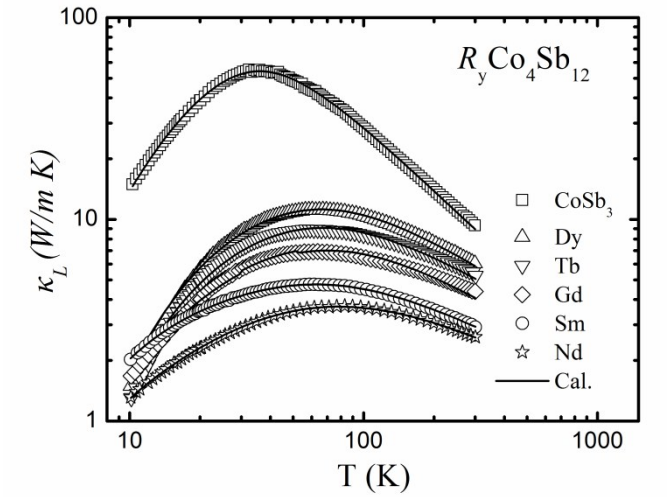

Fig. S6 Low-temperature lattice thermal conductivity κ_L from 10 to 300 K for $CoSb_3$ and $R_yCo_4Sb_{12}$ (R represents the fillers: Nd, Sm, Gd, Tb, and Dy). The solid lines are fitting curves based on Eq. (S1) and (S2).

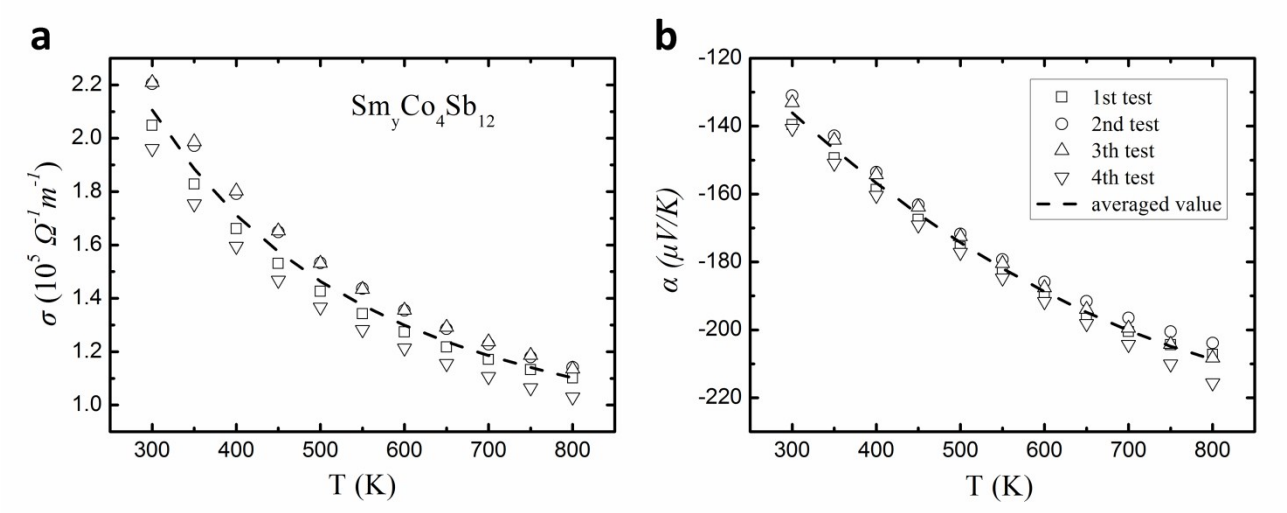

Fig. S7 Cycling measurements of (a) electrical conductivity σ and (b) Seebeck coefficient α for $Sm_yCo_4Sb_{12}$.

Table S1 Nominal composition, actual composition of the fillers (*R*) based on the EDS measurement, lattice parameter *a*, and room temperature lattice thermal conductivity κ_L, Hall carrier concentration *n*, electrical conductivity σ, Seebeck coefficient α, electron effective mass *m** and *zT* in $R_yCo_4Sb_{12}$ (*R* = Nd, Sm, Gd, Tb, Dy, and Tm).

Nominal Composition	Actual *R* Composition	*a* (Å)	κ_L (W/m·K)	*n* (10^{20} cm^{-3})	σ (10^5 $\Omega^{-1}m^{-1}$)	α (μV/K)	*m** (m_0)	*zT*
$Tm_{0.2}Co_4Sb_{12}$	---	9.034	6.8	0.08	0.04	-285	---	0.02
$Dy_{0.2}Co_4Sb_{12}$	0.017	9.035	5.1	0.25	0.23	-271	2.1	0.1
$Tb_{0.2}Co_4Sb_{12}$	0.029	9.036	4.6	0.37	0.36	-243	2.2	0.13
$Gd_{0.2}Co_4Sb_{12}$	0.036	9.038	4.1	0.61	0.54	-231	2.7	0.19
$Nd_{0.2}Co_4Sb_{12}$	0.148	9.046	2.1	3.35	1.64	-134	3.5	0.29
$Sm_{0.2}Co_4Sb_{12}$	0.154	9.048	2.4	3.59	2.11	-136	3.9	0.33

Table S2 Fitted parameter *L, A, B, C,* and ω_0 by Debye model for $CoSb_3$ and $R_yCo_4Sb_{12}$ (*R* = Dy, Tb, Gd, Nd, and Sm).

$R_yCo_4Sb_{12}$	*L* (μm)	*A* (10^{-43} s^3)	*B* (10^{-18} s/K)	*C* (10^{34} s^{-3})	ω_0 (cm^{-1})
$CoSb_3$	4.22	3.4	4.04	---	---
$Dy_{0.017}Co_4Sb_{12}$	1.04	24.1	3.11	1.69	72
$Tb_{0.029}Co_4Sb_{12}$	2.45	34.4	3.12	2.54	96
$Gd_{0.036}Co_4Sb_{12}$	2.00	45.0	3.63	3.53	172
$Nd_{0.148}Co_4Sb_{12}$	1.35	116	3.32	15.6	231
$Sm_{0.154}Co_4Sb_{12}$	1.97	127	3.08	16.7	320

Supplementary References

1 Y. Z. Pei, L. D. Chen, W. Zhang, X. Shi, S. Q. Bai, X. Y. Zhao, Z. G. Mei and X. Y. Li, *Appl. Phys. Lett.*, 2006, **89**, 221107.

2 L. D. Chen, T. Kawahara, X. F. Tang, T. Goto, T. Hirai, J. S. Dyck, W. Chen and C. Uher, *J. Appl. Phys.*, 2001, **90**, 1864-1868.

3 Y. Z. Pei, S. Q. Bai, X. Y. Zhao, W. Zhang and L. D. Chen, *Solid State Sci.*, 2008, **10**, 1422-1428.

4 X. Y. Zhao, X. Shi, L. D. Chen, W. Q. Zhang, S. Q. Bai, Y. Z. Pei and X. Y. Li, *Appl. Phys. Lett.*, 2006, **89**, 092121.

5 Y. Tang, S.-w. Chen and G. J. Snyder, *J. Materiomics*, 2015, **1**, 75-84.

6 V. L. Kuznetsov, L. A. Kuznetsova and D. M. Rowe, *J. Phys.: Condens. Matter*, 2003, **15**, 5035-5048.

7 J. Callaway, *Phys. Rev.*, 1959, **113**, 1046-1051.

8 J. Callaway and H. C. Baeyer, *Phys. Rev.*, 1960, **120**, 1149-1154.

9 D. T. Morelli, T. Caillat, J. P. Fleurial, A. Borshchevshy, J. W. Vandersande, B. Chen and C. Uher, *Phys. Rev. B*, 1995, **51**, 9622-9628.

10 Y. Jiang, X. P. Jia, L. Deng and H. A. Ma, *J. Rare Eerths*, 2012, **30**, 388-391.

11 Y. P. Jiang, B. Xu, L. Zhang, Y. Liu, D. Yu, Z. Liu, J. He and Y. Tian, *Mater. Lett.*, 2013, **98**, 171-173.